

DOI: 10.1002/cssc.201300585

A Method for Creating Microporous Carbon Materials with Excellent CO₂-Adsorption Capacity and Selectivity

Dan Qian, Cheng Lei, En-Min Wang, Wen-Cui Li, and An-Hui Lu^{*[a]}

A new synthetic approach for the fabrication of microporous carbon materials (HCMs) by using discrete chelating zinc species as dynamic molecular porogens to create extra micropores that enhance their CO₂-adsorption capacity and selectivity is reported. During the carbonization process, the evaporation of the in situ-formed Zn species would create additional nano-channels that contribute to the additional micropore volume for CO₂ adsorption. The resultant HCMs show an increased number of micropores, with sizes in the range 0.7–1.0 nm and a high CO₂-adsorption capacity of 5.4 mmol g⁻¹ (23.8 wt%) at 273 K and 3.8 mmol g⁻¹ (16.7 wt%) at 298 K and 1 bar, which are superior to those of most carbon-based adsorbents with N-


doping or high specific surface areas. Dynamic gas-separation measurements, by using 16% CO₂ in N₂ (v/v) as a feedstock, demonstrated that CO₂ could be effectively separated from N₂ under ambient conditions and shows a high separation factor ($S_{\text{CO}_2/\text{N}_2} = 110$) for CO₂ over N₂, thereby reflecting a strongly competitive CO₂-adsorption capacity. If the feedstock contained water vapor, the dynamic capacity of CO₂ was almost identical to that measured under dry conditions, thus indicating that the carbon material had excellent tolerance to humidity. Easy CO₂ release could be realized by purging an argon flow through the fixed-bed adsorber at 298 K, thus indicating good regeneration ability.

Introduction

The increasing concentration of CO₂ in the atmosphere might contribute to apparent global warming and serious climate change.^[1] On the other hand, CO₂ is a renewable and ubiquitous carbon source for the production of MeOH and dimethyl ether, which are efficient alternative transportation fuels, as well as their various derivatives.^[2] Furthermore, the sequestration of low-partial-pressure CO₂ from an enclosed space is of importance in life-support systems for submarines and in space.^[3] Hence, the selective capture and separation of CO₂ in an economical and energy-efficient fashion is of positive significance, not only to the academic community but also for social and economic progress.^[4] As a promising alternative to liquid-amine- and ammonia-adsorption processes, CO₂ adsorption onto porous adsorbents, including metal-organic frameworks (MOFs),^[5] amine-functionalized silica,^[6] zeolites,^[7] carbon materials,^[8] and porous polymers,^[9] has been investigated extensively. Among these adsorbents, porous carbon materials are believed to be among the most promising candidates for carbon capture, owing to their low cost, high surface area, excellent thermal and chemical stability, ease of preparation and regeneration, and high amenability to pore-structure tailoring and

surface functionalization.^[10] Nevertheless, most activated carbon materials exhibit low CO₂-adsorption capacities,^[3a,4a,11] which render them unsuitable for this application. To improve the CO₂-adsorption capacity of porous carbon materials, great effort has been directed towards enhancing the adsorbate-adsorbent interactions and storage space through functionalizing the active surface or enlarging the specific surface area of an adsorbent.^[12] For example, Monte and co-workers recently reported the fabrication of N-enriched porous carbon materials (N content: 5%, Brunauer-Emmett-Teller surface area: $S_{\text{BET}} = 666 \text{ m}^2 \text{ g}^{-1}$) that showed a maximum CO₂-adsorption capacity of 3.29 mmol g⁻¹ at 298 K and 1 bar through the carbonization of a polymeric material by using deep eutectic solvents as both precursors and structure-directing agents at 800 °C.^[8d] A porous carbon monolith (N content: 1.92%, $S_{\text{BET}} = 467 \text{ m}^2 \text{ g}^{-1}$) has been prepared by using lysine as both a catalyst and a nitrogen source, which showed a maximum CO₂-adsorption capacity of 3.13 mmol g⁻¹ at 298 K and 1 bar.^[3] In addition to the aforementioned nitrogen-doped porous carbon materials that showed enhanced affinity for CO₂ molecules, porous carbon materials prepared with high specific surface areas (SSAs) exceeding 2000 m² g⁻¹ have also exhibited high CO₂-adsorption capacities at atmospheric pressure.^[4b,13] For example, a nano-structured templated carbon TC-EMC material with a high surface area ($S_{\text{BET}} = 3840 \text{ m}^2 \text{ g}^{-1}$) has been prepared by using zeolite EMC-2 as a hard template through chemical vapor deposition (CVD) and its CO₂-adsorption capacity was 3.3 mmol g⁻¹ at 298 K and 1 bar.^[14] Recently, a new type of hierarchical porous carbon monolith ($S_{\text{BET}} = 2160 \text{ m}^2 \text{ g}^{-1}$) was derived from surfactant-templated poly(benzoxazine-co-resol) polymers and subsequently activated by a CO₂ stream. The monolith exhibited

[a] D. Qian, C. Lei, E.-M. Wang, Prof. W.-C. Li, Prof. A.-H. Lu
State Key Laboratory of Fine Chemicals
School of Chemical Engineering
Faculty of Chemical, Environmental and
Biological Science and Technology
Dalian University of Technology
Dalian, 116024 (PR China)
E-mail: anhuilu@dlut.edu.cn

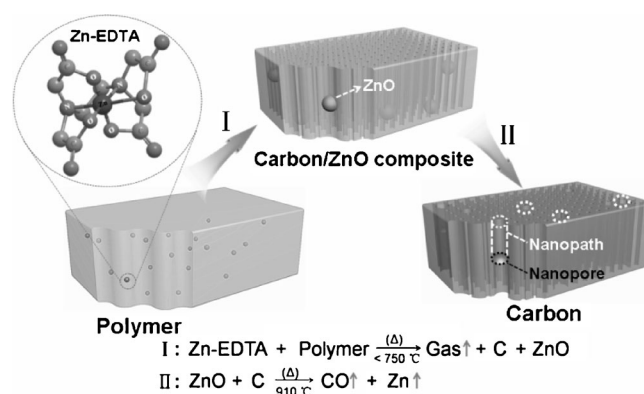
 Supporting Information for this article is available on the WWW under <http://dx.doi.org/10.1002/cssc.201300585>.

a high CO₂ uptake of 3.30 mmol g⁻¹ at 298 K and 1 bar.^[4b] To increase the CO₂-adsorption capacity, in particular at low CO₂ partial pressures, several groups have explored the chemical activation of activated carbon materials that contained a large proportion of additional micropores and unavoidably enlarged pores (which are unfavorable for CO₂ adsorption).^[8b, 15] For example, Fuertes and co-workers recently reported a maximum CO₂-adsorption capacity of 4.8 mmol g⁻¹ at 298 K and 1 bar for a sawdust-based porous carbon material (AS-2-600).^[8b] Wahby and co-workers demonstrated that a carbon material produced by the chemical activation of petroleum pitch exhibited a high surface area and a high CO₂-adsorption capacity of 4.7 mmol g⁻¹ at 298 K and 1 bar.^[15b] These results clearly demonstrate that moderate chemical activation may be a feasible way of producing porous carbon materials with high CO₂-adsorption capacities. However, an additional activation method is always energetically unfavorable and leads to a low yield of the carbon material. In general, pores with sizes of less than 1.0 nm greatly contribute to the CO₂-adsorption capacity of a porous carbon material.^[16] Recent studies have shown that porous carbon materials with a large population of pores with sizes between 0.7 and 1.0 nm exhibited a larger CO₂-adsorption performance than those with large micropores.^[8a, 12i, 16, 17] Hence, it is a challenge to develop a new and straightforward synthesis of porous carbon materials with abundant micropores, in particular pore sizes of less than 1.0 nm.

Inspired by these studies and on the basis of our previous work, we wanted to develop a new approach for the preparation of porous carbon materials with enhanced microporosity (typical pore sizes of 0.7–1.0 nm) by introducing molecular porogens, including organic chelating agents, which not only homogeneously mix with the carbon precursor, but also coordinate inorganic cations (e.g., Zn²⁺) on the atomic level. We expected that, during the carbonization process, the decomposition of chelating agents can lead to the formation of molecular-sized micropores. Moreover, the presence of spatially nearby inorganic cations can sinter in situ and form small clusters, which, in turn, are isolated by the surrounding carbon species.^[18] Further high-temperature treatment would result in evaporation of the Zn clusters, thereby forming micropores that include the nanospace in which the ZnO clusters sat and the nanochannel through which the Zn is volatilized. Under these conditions, we established a simple synthesis of porous carbon materials with an enlarged microporous surface area and narrow micropore sizes of 0.7–1.0 nm. These carbon materials show significant high CO₂-capture capacity (5.4 mmol g⁻¹ at 273 K and 3.8 mmol g⁻¹ at 298 K, 1 bar) and high tolerance to moisture and, thus, are promising candidates for gas adsorption and separation.

Results and Discussion

The overall process for the synthesis of microporous carbon materials is shown in Scheme 1 (for details, see the Experimental Section). The first step in the synthesis of the microporous carbon materials is the preparation of the carbon precursors, that is, the polymer monoliths (HCM-p). The polymer mono-



Scheme 1. Principles in the synthesis of the microporous carbon material by using zinc species as dynamic molecular porogens for the creation of abundant microporosity.

liths were synthesized by the copolymerization of resorcinol and formaldehyde in the presence of imidazole as a catalyst and zinc chloride (ZC) as a molecular porogen to impart extra microporosity; EDTA was added as a chelating agent to uniformly disperse the Zn ions over the HCM-p. After sequentially adding the reactants and aging at 90 °C for 4 h, a homogenous gel was obtained (see the Supporting Information, Figure S1). Notably, if the synthesis was performed in the same manner as that of HCM-p-ZC-1 but without EDTA, it resulted in the formation of a flocculate product rather than a homogenous gel (see the Supporting Information, Figure S1). This result indicated that the use of EDTA in the synthesis was crucial for obtaining a homogenous gel. A porous carbon monolith (HCM) with abundant micropores was obtained by carbonization of the polymer at 910 °C under a nitrogen atmosphere, based on the pore-evolution process (stages I and II) shown in Scheme 1. In stage I, accompanied by decomposition of the polymer and the chelating agent, conventional micropores emerged and highly dispersive ZnO clusters grew and became embedded in the carbon matrix. During stage II, as the temperature increased, the ZnO clusters were reduced to Zn and then vaporized, which led to the creation of incremental microporous pathways, thereby adding micropore volume for CO₂ adsorption.

Photographs (Figure 1a and b) showed that both the synthesized polymer and its corresponding carbon product exhibited a monolithic shape. A carbonization process led to linear shrinkage of 21% and volume shrinkage of 58%, with a bulk density of about 0.23 cm³ g⁻¹. SEM was used to image the microscopic morphology of the as-prepared carbon material. The SEM image (Figure 1c) indicated that the skeleton of the carbon monoliths consisted of homogeneously interconnected spherical units.

To investigate the thermal decomposition of the polymer (HCM-p), thermal analysis from 40 to 950 °C was performed with a heating rate of 10 °C min⁻¹ under a nitrogen atmosphere (Figure 1d). After the decomposition process, the yield of carbon was almost 51%, thus indicating that HCM-p could be effectively converted into carbon. Essentially, the thermogravimetry (TG) curve involved three weight-loss steps: The

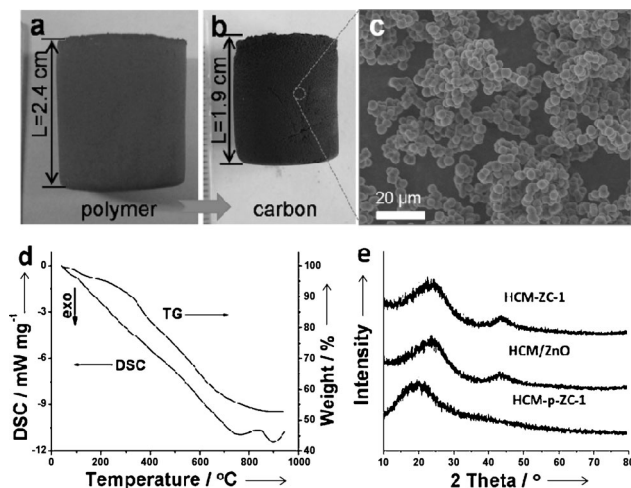


Figure 1. Photographs of a) the polymer monolith and b) its corresponding carbon monolith. c) SEM image of HCM-ZC-1. d) TG and DSC curves of HCM-p. e) XRD patterns of HCM-p-ZC-1, HCM/ZnO, and HCM-ZC-1.

first structural evolution, within the temperature range 40–300 °C, was mainly attributed to the release of H₂O, CO₂, CO, and other gases, which originated from the decomposition of the organic substance.^[20] During the carbonization process, HCM/ZnO composites were formed, owing to decomposition of the polymer and the chelated Zn ions, between 400–700 °C. At carbonization temperatures over 750 °C, the ZnO clusters were reduced to metallic Zn through carbothermic reduction, ZnO + C → Zn₍₀₎ + CO_(g) ($\Delta H_1 < 0$). Subsequently, on increasing the temperature to 910 °C, the Zn metal clusters (boiling point: 908 °C) were vaporized, along with the inert gases, Zn₍₀₎ → Zn_(g) ($\Delta H_2 < 0$), as clearly shown by the appreciably steep gradients in the differential scanning calorimetry (DSC) curve at 750 and 900 °C.^[21]

To determine the changes in the Zn species during the different stages of the carbonization process, HCM-p, the corresponding carbon materials (HCM), and HCM/ZnO were subjected to treatment in air at 700 °C for 2 h and the final residues were collected. The residual mass percentages are listed in Table 1. Based on the elemental composition (C, H, O, N, and Zn) of the initial reactant and the boiling point of ZnO (about 1800 °C), we deduced that the solid residue after calcination of HCM-p, HCM, and HCM/ZnO at 700 °C was ZnO. Thus, the residues (ZnO) were observed in the polymer samples if a zinc precursor was used during the synthesis and the mass percentage of ZnO in HCM-p increased with increasing amount of ZnCl₂. Nevertheless, no detectable residue was left on calcination of the corresponding carbon samples (HCMs) at 700 °C, except for the composite (HCM/ZnO). This result confirmed that Zn had escaped from the carbon matrix through the reduction of ZnO to Zn and then evaporation during the high-temperature carbonization process (910 °C). Furthermore, the amount of the residue in HCM-p was roughly coincident with the addition of the Zn source during synthesis.

To confirm that the porogens were highly dispersed and that the ZnO clusters were nanosized, we measured the XRD patterns of HCM-p-ZC-1 and of the carbon products derived

Table 1. Mass percentages of the residues derived from HCM-p and HCMs after calcination at 700 °C in air.

Polymer ^[a]	Residue mass percentage ^[b] [wt %]	Carbon ^[c]	Residue mass percentage ^[b] [wt %]
HCM-p-ZC-0	none	HCM-ZC-0	none
HCM-p-ZC-0.5	1	HCM-ZC-0.5	none
HCM-p-ZC-1	3	HCM-ZC-1	none
HCM-p-ZC-1'	3	HCM-ZC-1'	none
HCM-p-ZC-2	6	HCM-ZC-2	none
HCM-p-ZC-1	3	HCM/ZnO ^[d]	4
HCM-p-ZC-1-R ^[e]	7	HCM-ZC-1-R	none

[a] Polymer monoliths (HCM-p) prepared by copolymerization and washing before carbonization. [b] Approximate value. [c] Final carbon monolith products (HCMs) after the carbonization of HCM-p at 910 °C for 5 h. [d] HCM/ZnO was obtained by the carbonization of HCM-p-ZC-1 at 750 °C. [e] HCM-p-ZC-1-R represents the sample derived from the polymer monolith without washing with water.

from the carbonization of HCM-p-ZC-1 at 750 °C (HCM/ZnO) and 910 °C (HCM-ZC-1). As shown in Figure 1 e, the characteristic peaks at about 31.7°, 36.3°, and 47.5°, which were assigned to ZnO, and the peaks at 26.7°, 38.9°, 43.3°, which were assigned to metallic zinc, were absent in the XRD patterns of HCM-p-ZC-1, HCM/ZnO, and HCM-ZC-1. However, energy-dispersive X-ray spectroscopy (EDX) of the elements in the HCM/ZnO composite showed a concordance of the signals of Zn, C, and O, thus suggesting the existence and uniform distribution of Zn and O elements (see the Supporting Information, Figure S2). On the basis of the XRD and EDX results, we concluded that the molecular porogens were uniformly dispersed in the polymer monolith and that the formed ZnO clusters were also highly dispersed. On increasing the carbonization temperature to 910 °C, the centrally interlocked Zn clusters, which were derived from the reduction of the ZnO, vaporized and created extra micropores, including nanopores and nanochannels in the carbon skeleton, in which the ZnO sat and through which Zn passed, respectively.

The N₂-adsorption isotherms of HCMs and HCM/ZnO at 77 K are shown in Figure 2 a; the textural parameters are summarized in Table 2. All of the HCM samples show type-I isotherms, thus suggesting dominant microporous characteristics. Remarkably, the HCM-ZC-1 sample prepared with zinc chloride showed a high surface area of 808 m²g⁻¹, which was 66% and 32% higher than those of HCM-ZC-0 prepared without zinc chloride and HCM/ZnO carbonized at 750 °C. Notably, the presence of only 3 wt% of ZnO (equal to 2.3 wt% Zn²⁺) in a polymer matrix afforded an addition 60% micropore volume, which would contribute to the high CO₂-adsorption capability of the carbon materials. This fascinating result mainly stemmed from the as-formed nanochannels (micropores), which were derived from the volatilized zinc clusters. In contrast, carbon material HCM-ZC-1', which was derived from HCM-p-ZC-1' without EDTA, only had a 28% higher porosity than HCM-ZC-0 (see the Supporting Information, Figure S3), owing to the formation of a nonuniform gel in the absence of EDTA. In this aspect, we can draw the conclusion that molecular porogens that contain an organic chelating agent and an inorganic zinc

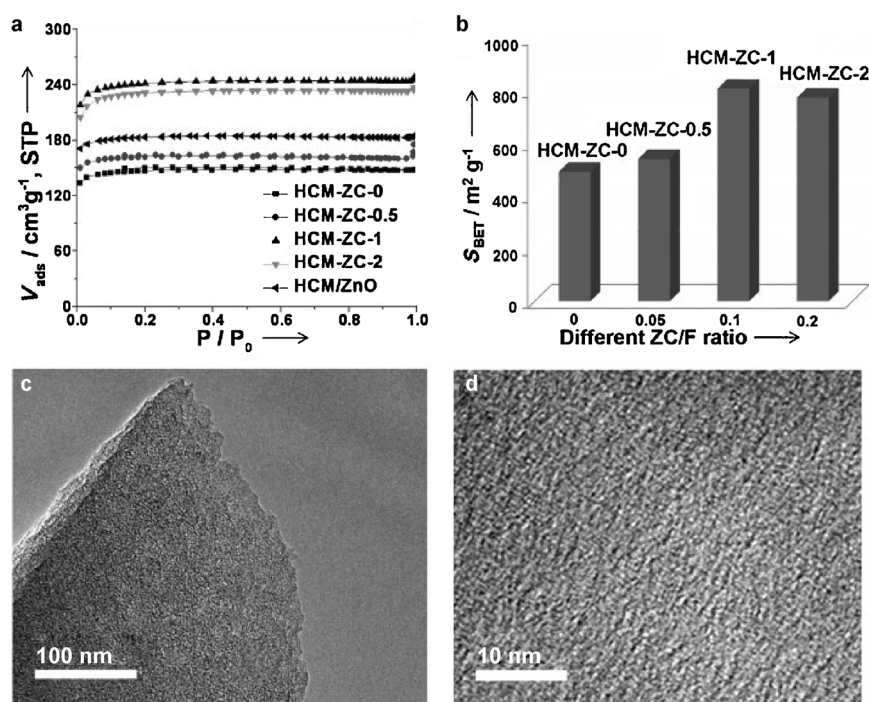


Figure 2. a) Nitrogen-sorption isotherms of the HCMs and b) the correlation between the amount of ZnCl₂ used and the specific surface areas. c, d) TEM images of HCM-ZC-1.

Table 2. Pore parameters and CO₂ uptake of the porous carbon materials.

Sample	Pore parameters ^[a]		CO ₂ uptake@1 bar [mmol g ⁻¹]		Q _{st} [kJ mol ⁻¹]
	S _{BET} [m ² g ⁻¹]	V _{total} [cm ³ g ⁻¹]	273 K	298 K	
HCM-ZC-0	492	0.23	4.0	2.9	26.3
HCM-ZC-0.5	541	0.27	4.1	2.9	26.0
HCM-ZC-1	808	0.38	5.4	3.8	22.2
HCM-ZC-1'	629	0.32	4.0	2.9	27.3
HCM-ZC-2	774	0.37	4.4	3.0	22.0
HCM/ZnO	612	0.29	4.3	3.0	24.7
HCM-ZC-1-R	540	0.27	3.9	2.8	24.8

[a] The values were derived from the N₂-sorption isotherms at 77 K.

salt efficiently facilitate the development of micropores through decomposition of the chelating agent and evaporation of the in situ generated Zn clusters.

Figure 2b shows the relationship between the BET surface area and the amount of Zn used. In general, the use of a larger amount of zinc chloride leads to high porosity. However, the use of too large an amount of zinc chloride led to a decrease in BET surface area, as reflected for samples HCM-ZC-2 and HCM-ZC-1-R, which showed a BET surface area only 67% of that of HCM-ZC-1 (for details, see the Supporting Information, Figure S4). The TEM images of HCM-ZC-1 (Figure 2c and d and the Supporting Information, S5) reveal that the carbon skeleton is homogeneous and consists of micropores, with no detectable larger pores. This result is consistent with the nitrogen-sorption analysis. In addition, the proportion of the microporous surface area is high and typically reaches more than

90% of the total surface area, thus indicating that the microporosity is greatly enlarged.

Encouraged by the optimized microporosity results, we performed CO₂-adsorption measurements at 273 and 298 K and recorded CO₂-adsorption isotherms (Figure 3a,b). The CO₂-capture capacities are listed in Table 2. At about 1 bar, HCM-ZC-1 showed a high CO₂-adsorption capacity of 5.4 mmol g⁻¹ (equivalent to 23.8 wt% of the adsorbent mass) at 273 K and 3.8 mmol g⁻¹ (16.7 wt%) at 298 K. Such excellent CO₂-adsorption performance is comparable to those of recently reported carbon and MOF materials (see the Supporting Information, Table S1). In addition, taking into account the number of CO₂ molecules adsorbed per m² (based on the microporous surface area, at 273 K), we estimated a value of $7.4 \times 10^{-6} \text{ mol m}^{-2}$ (i.e., 4.4 CO₂

molecules per nm²) for HCM-ZC-1. This result surpasses the performance of all other carbon materials known so far and clearly shows a full occupation of CO₂ molecules on the micropore surface of this sample. As observed from the CO₂-adsorption isotherms, HCM-ZC-1 exhibited much higher CO₂ uptake than HCM-ZC-0 and HCM-ZC-1', owing to its improved dominant microporosity (Figure 3 and the Supporting Information, S3). Therefore, in this regard, the incorporation of zinc resulted in the creation of significant additional microporosity (small micropores) to facilitate the adsorption of a considerable amount of CO₂. This result was consistent with previous reports, in which porous carbon materials derived from Zn-containing MOF-5, IRMOFs, and ZIF-8 displayed exceptional porosity and narrow pore sizes.^[22]

To determine the strengths of the interactions between CO₂ molecules and the skeleton of the carbon materials, the CO₂-adsorption energy (isosteric heat of adsorption, Q_{st}) was calculated by measuring the CO₂-adsorption isotherms at 273 and 298 K, based on a variant of the Clausius–Clapeyron equation. The plots of Q_{st} as a function of CO₂ uptake for all of the carbon samples are shown in Figure 4. The initial isosteric heats of adsorption for these carbon materials varied within the range 20–33 kJ mol⁻¹ at low CO₂ uptake, which were lower than previously reported values for typical N-doped carbon adsorbents.^[1b,4a] The low Q_{st} values of CO₂ adsorption on the HCMs characterize the weak interactions between CO₂ and the carbon hosts, thereby resulting in a relatively simple desorption process and fast adsorption/desorption rates.

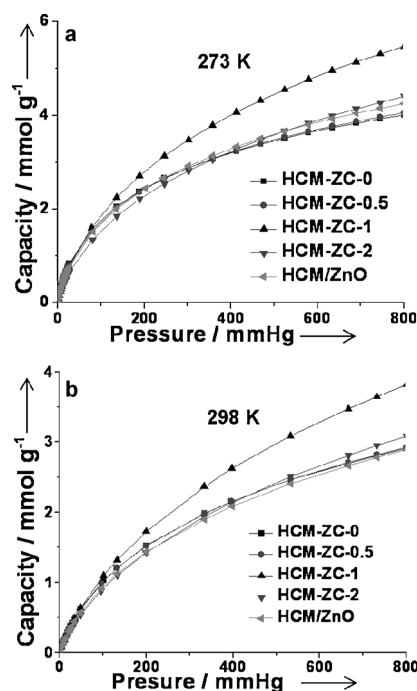


Figure 3. CO₂-adsorption isotherms of the microporous carbon materials at a) 273 K and b) 298 K.

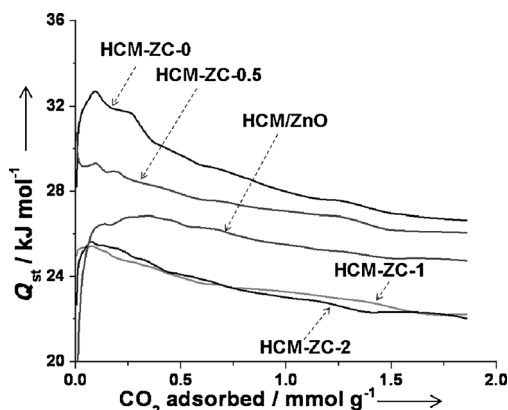


Figure 4. Isothermic heat of CO₂ adsorption of the microporous carbon materials.

The sorption process of CO₂ on microporous carbon materials is predominantly associated with Van der Waals forces and electrostatic forces.^[23,24] Considering the kinetic diameter of a CO₂ molecule (3.3 Å), high-performance adsorbents for CO₂ capture should possess intrinsic properties, such as an abundance of micropores and suitable pore sizes. Because the surface areas of the micropores, in particular of ultrafine micropores, are particularly important, we validated the pore-size distributions by using DFT, based on the CO₂-adsorption data at 273 K. The resultant DFT pore-size distributions and cumulative surface areas are shown in Figure 5. HCM-ZC-0 shows a slightly higher cumulative microporous surface area than HCM-ZC-1 if the micropore sizes are less than 0.7 nm; this value is roughly twice the kinetic diameter of a CO₂ molecule.

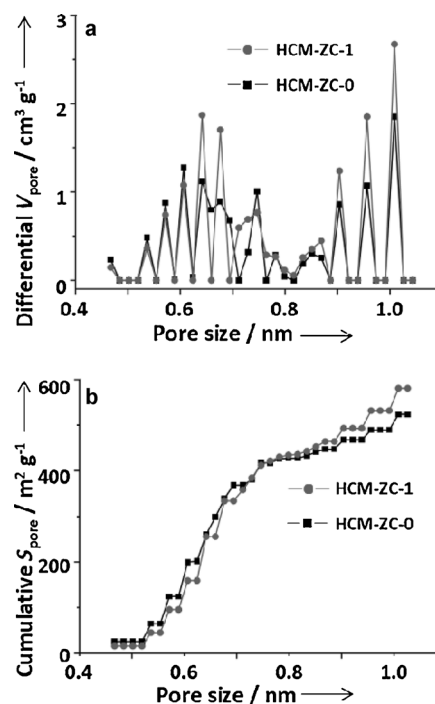


Figure 5. a) PSDs and b) accumulated microporous surface areas of HCM-ZC-0 and HCM-ZC-1. The data were calculated from the CO₂-adsorption data at 273 K by using DFT.

Moreover, the microporous surface area of HCM-ZC-1 is 10.9% larger than that of HCM-ZC-0 if the micropore size is above 0.7 nm. This result further confirms the effect of Zn in enlarging the pore volume and micropore size. Based on the N₂-adsorption results, we conclude that the extra microporous surface area in HCM-ZC-1 is attributed to micropores with pores larger than 0.7 nm but smaller than 1 nm, whereas the volume of ultrafine micropores (less than 0.7 nm) is not or minimally influential. These results reveal that the adsorption behavior is largely governed by the actual microporous surface areas and micropore sizes.

The adsorption kinetics of CO₂ over HCM-ZC-1 were determined in a thermogravimetric system with a mixed stream of 83% CO₂ and 17% N₂ (v/v) at 27 °C (see the Experimental Section). The Supporting Information, Figure S6a, shows the mass changes in HCM-ZC-1 during the adsorption and desorption processes. The mass of the loaded sorbent is represented relative to the initial mass of the sorbent. After introducing CO₂ gas, a fast weight increase to about 107 wt% was observed (see the Supporting Information, Figure S6b). Then, the adsorption rate decelerated and tended to remain constant; the total mass approached a steady state of about 110.5 wt% (2.4 mmol g⁻¹), which was lower than, as a rough estimation, the static adsorption capacity value (3.8 mmol g⁻¹). This phenomenon may indicate that the adsorption kinetics of CO₂ molecules in the narrow micropores of HCM-ZC-1 are limited during a dynamic adsorption process.

Subatmospheric pressures are a particular challenge for gas separation. Thus, we performed dynamic breakthrough separation experiments to determine the CO₂-separation perfor-

mance of HCM-ZC-1.^[25] A mixed stream of 16% (v/v) CO₂ in N₂ was used to simulate flue gas. Thus, HCM-ZC-1 (0.867 g) was placed in a column with a length of 130 mm and an internal diameter of 8 mm. As shown in Figure 6a, the breakthrough

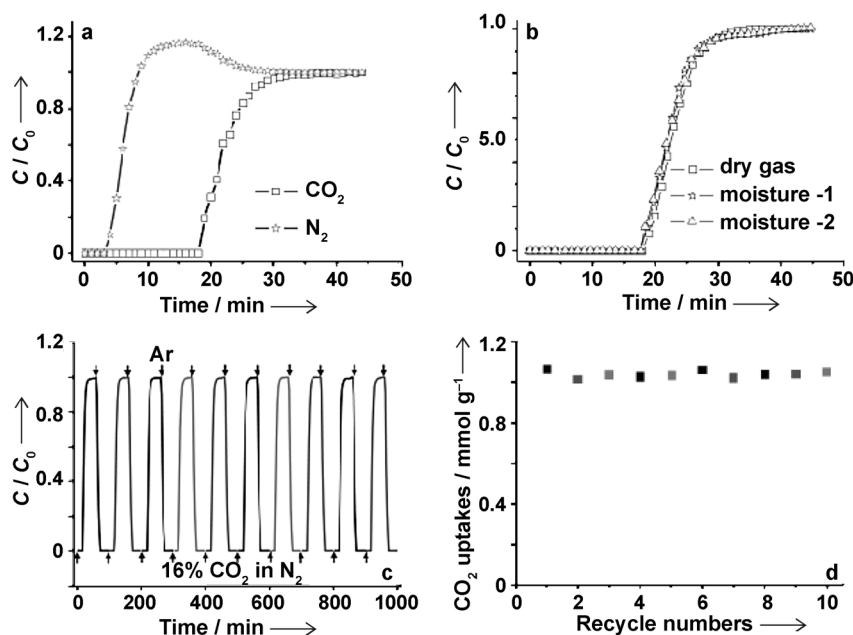


Figure 6. a) Breakthrough curve of HCM-ZC-1 by using a stream of 16% CO₂ in N₂ (v/v) at 25 °C. b) Breakthrough curve of CO₂ under moisture conditions. c) Recycling runs of CO₂-adsorption/desorption on HCM-ZC-1 at 25 °C by using a stream of 16% CO₂ in N₂ (v/v), followed by regeneration under a flow of argon. d) CO₂ uptake of each adsorption run.

curve can be divided into three stages: Stage 1 (0–5 min), in which both CO₂ and N₂ were captured because the sorbent was not saturated with CO₂ and N₂. Stage 2 (5–30 min), in which CO₂ was still captured by the adsorbent, whereas no more N₂ was captured because the adsorbent was saturated with N₂. In addition, because the adsorbent competitively/preferentially tended to capture CO₂, some of the preadsorbed N₂ molecules were expelled into the effluent stream by CO₂ molecules; this expulsion explains why an extra N₂ stream was observed in the effluent stream. Such a phenomenon strongly shows that HCM-ZC-1 can selectively capture CO₂ from N₂. Stage 3 (>30 min), in which the adsorbent was saturated with both CO₂ and N₂; thus, the flow rate and composition of the effluent stream were the same as those of the feed stream.

According to the breakthrough curve, the calculated CO₂ mass capacity of HCM-ZC-1 is about 1.05 mmol g⁻¹, which is coincident with the single-component CO₂-adsorption value (1.1 mmol g⁻¹) at a CO₂ partial pressure of 151 mbar (1 mbar = 1.33 mmHg). The N₂ mass-uptake capacity is 0.05 mmol g⁻¹. The separation factor, $S_{\text{CO}_2/\text{N}_2}$, for CO₂ over N₂, is estimated to be 110 as calculated according to the formula $S_{\text{CO}_2/\text{N}_2} = [q_{\text{CO}_2}/y_{\text{CO}_2}]/[q_{\text{N}_2}/y_{\text{N}_2}]$, in which q_{CO_2} and q_{N_2} are the amounts of adsorbed of CO₂ and N₂, respectively, and y_{CO_2} and y_{N_2} are the mole fractions of CO₂ and N₂ in the gas phase, respectively.

Commonly, the separation efficacy of a physisorbent (e.g., zeolites, MOFs, etc.) decreases under humid conditions. To ex-

amine the performance of our microporous carbon material, we further tested its CO₂-sorption and -separation capability under humid conditions by using a gas mixture of CO₂/N₂/H₂O (14:83.5:2.5, v/v/v). The breakthrough results, as shown in Figure 6b, show that HCM-ZC-1 can

induce the complete separation of CO₂ from the stream of N₂ and H₂O. The calculated dynamic capacity of CO₂ is about 1.0 mmol g⁻¹, which is almost identical to that recorded under dry conditions. The measurements were repeated twice and all resulted in almost-identical results.

To ascertain the recyclability of HCM-ZC-1 in CO₂ sorption, gas-cycling experiments at 298 K were performed over ten cycles (Figure 6c). The CO₂-saturated composite was subjected to a purge with argon gas at a flow rate of 20 mL min⁻¹ at 25 °C. After approximately 20 min, no CO₂ was detected in the effluent stream. Successive regeneration experiments showed that HCM-ZC-1 retained >95% of its intrinsic capacity after mild regeneration (Figure 6d). Further cycling did not lead to a visible decrease

in capacity. These results signify that HCM-ZC-1 provided a high-capacity separation with very mild conditions for regeneration. Hence, the dynamic results also confirm that the HCM-ZC-1 composite is extremely selective for adsorbing CO₂ over N₂ and represents a major advance in CO₂-separation capacity. This result indicates that porous carbon materials can be good adsorbents, owing to the high CO₂-adsorption capacity and high CO₂/N₂ selectivity.

Conclusions

Porous carbon materials with enlarged microporosities were prepared by using molecular porogens (e.g., zinc chloride and ethylene diamine tetraacetic acid). During the carbonization process, the evaporation of the in situ formed Zn clusters created additional microporous pathways that contributed to the additional micropore volume for CO₂ adsorption. The obtained porous carbon materials showed a high CO₂-adsorption capacity of 5.4 mmol g⁻¹ (23.8 wt%) at 273 K and 3.8 mmol g⁻¹ (16.7 wt%) at 298 K, 1 bar. Consistent with the pure-gas-adsorption results at a CO₂ partial pressure of 151 mbar and at room temperature, HCM-ZC-1 exhibited a high CO₂ uptake of about 1.05 mmol g⁻¹ with 16% CO₂ in N₂ (v/v) as a feedstock for dynamic adsorption. Moreover, the high separation factor of >100 for the capture of CO₂ over N₂, simple regeneration ability, and superior moisture resistance afforded HCM-ZC-

1 the potential for meeting the needs of the CO₂-adsorption economy. Compared with carbide-derived carbons (CDCs), Ti/C, and other chemically activated carbon materials, our porous carbon material shows advantages in terms of high carbonization yield, high CO₂-capture capacity, high separation selectivity, and easy handling and regeneration, which are desirable and indispensable properties for practical CO₂-capture applications.

Experimental Section

Chemicals

Resorcinol (99.5%) and formaldehyde (37 wt% solution) were purchased from Tianjin Kernel Chemical Reagent Co., Ltd. Zinc chloride (98.5%), EtOH (99.7%), imidazole (99.5%), ethylene diamine tetraacetic acid (99.0%), and formalin (37 wt%) were all purchased from Sinopharm Chemical Reagent Co., Ltd. All chemicals were used as received.

Synthesis of the porous carbon materials

The carbon precursors, that is, the polymer monoliths (HCM-p), were synthesized by the copolymerization of resorcinol (R) and formaldehyde (F) in the presence of imidazole (IM) as the catalyst. To impart extra microporosity, zinc chloride (ZC), was added into the polymerization system. In a typical synthesis, resorcinol (30 mmol) was dissolved in water (15 mL) to form a clear solution. Afterwards, IM (6 mmol), ethylene diamine tetraacetic acid (EDTA, 1.5 mmol), and zinc chloride (ZC, 6 mmol) were sequentially added to the solution with vigorous stirring. Subsequently, formalin (37 wt%) that contained formaldehyde (60 mmol, denoted as F) was quickly injected into the solution with fast stirring. Then, the clear solution (pH ≈ 5) was sealed and transferred into an oven at 90 °C. The solution quickly turned brown and solidified within 20 min to form a monolithic polymer gel. This gel was cured for an additional 4 h at 90 °C. The resultant HCM-p monolith was immersing in deionized water at 50 °C for 2 h to remove any unreacted reactant. This washing procedure was repeated five times to make sure that the Zn species had dispersed appropriately and that there were no free Zn species in the HCM-p monolith. Then, the washed polymer monolith was dried at 50 °C for 24 h in air. The porous carbon monolith (HCM) was obtained by carbonization of the polymer at 910 °C for 5 h under a nitrogen atmosphere.

The porous carbon products with different ZC/F ratios (ZC/F = 0:1, 0.05:1, 0.1:1, and 0.2:1) were denoted as HCM-ZC-0, HCM-ZC-0.5, HCM-ZC-1, and HCM-ZC-2, respectively. To preserve ZnO in the carbon matrix, HCM-p with ZC/F = 0.1:1 was also pyrolyzed at 750 °C for 7 h and the resultant sample was named HCM/ZnO. The sample derived from the polymer monolith without washing with water was named HCM-ZC-1-R (its preparation procedure was the same as that of HCM-ZC-1 in all other respects).

Characterization

The thermal decomposition behavior of the samples was monitored on a simultaneous thermal analyzer (Netzsch STA 449 F3) from 40 to 950 °C under a nitrogen atmosphere at a heating rate of 10 °C min⁻¹. Nitrogen-sorption experiments were performed at 77 K on a Micromeritics TriStar 3000 instrument. Before the measurements, the samples were evacuated at 200 °C for 6 h. The X-ray diffraction (XRD) measurements were performed on a Rigaku D/

Max 2400 diffractometer by using CuK_α radiation (40 kV, 100 mA, λ = 1.5406 Å). The Brunauer–Emmett–Teller (BET) method was used to calculate the specific surface areas (S_{BET}). The surface areas of the micropores (S_{micro}) were calculated by using the t-plot method. The pore-size distribution (PSD) of a carbon sample was calculated by fitting the isotherms calculated by DFT to experimental CO₂-adsorption isotherms at 0 °C.^[26] SEM investigations were performed on a Hitachi S-4800 instrument. TEM analyses were performed on a Tecnai G²20S-Twin equipment operating at 200 kV. The samples for TEM analysis were prepared by placing a droplet of the products in EtOH onto carbon-coated copper grids and drying at RT.

Equilibrium gas-adsorption measurements

The CO₂-adsorption isotherms were measured on a Micromeritics ASAP 2020 static volumetric analyzer at 25 and 0 °C. Prior to each adsorption experiment, the sample was degassed for 2 h at 200 °C to ensure that the residual pressure fell below 5 × 10⁻³ mbar. Then, the sample was cooled to RT and CO₂ was introduced into the system. The CO₂-adsorption capacity was recorded in terms of adsorbed volume under standard temperature and pressure (STP).

Kinetics of CO₂ adsorption

The adsorption kinetics of CO₂ were measured on a thermogravimetric analyzer (Netzsch STA 449 F3). For the analysis, the sample (about 10 mg) was degassed in a stream of N₂ (50 mL min⁻¹) at 200 °C for 1 h. Then, the sample was cooled in a N₂ stream to 27 °C and exposed to a gas stream that contained CO₂ (50 mL min⁻¹) and N₂ (10 mL min⁻¹) as a protective gas. After reaching a steady state, the sample was heated stepwise to 40, 50, and 70 °C and held at each temperature for 60 min. The mass of the sorbent plus the adsorbate was measured at each steady state.

Dynamic gas-separation measurements

The separation of CO₂ from CO₂/N₂ binary mixtures was performed on a fixed-bed adsorber (a stainless steel tube with an inner diameter of 8 mm and a length of 130 mm) at about 1 bar and 298 K, which were controlled by a pressure controller and a thermostatic water bath, respectively. First, the bed was heated at 95 °C in Ar at a flow rate of 50 mL min⁻¹ for 2 h. Then, the breakthrough experiment was performed by abruptly switching from Ar to the gas mixture that contained 16% CO₂ in N₂ (v/v) with a total flow rate of 7 mL min⁻¹. The effluent gas was monitored online by using an Agilent 7890A gas chromatograph with a thermal conductivity detector (TCD).

Acknowledgements

The project was supported by the Special Program for Basic Research of the Ministry of Science and Technology (2012CB626802), the State Education Ministry, and the PhD Programs Foundation (20100041110017) of the Ministry of Education of China, the Fundamental Research Funds for the Central Universities.

Keywords: adsorption • gas separation • microporous materials • porogens • zinc

- [1] a) D. M. D'Alessandro, B. Smit, J. R. Long, *Angew. Chem.* **2010**, *122*, 6194–6219; *Angew. Chem. Int. Ed.* **2010**, *49*, 6058–6082; b) Y. D. Xia, R. Mokaya, G. S. Walker, Y. Q. Zhu, *Adv. Energy Mater.* **2011**, *1*, 678–683.
- [2] a) T. Sakakura, J. C. Choi, H. Yasuda, *Chem. Rev.* **2007**, *107*, 2365–2387; b) C. S. Song, *Catal. Today* **2006**, *115*, 2–32.
- [3] G. P. Hao, W. C. Li, D. Qian, A.-H. Lu, *Adv. Mater.* **2010**, *22*, 853–857.
- [4] a) D. Qian, C. Lei, G. P. Hao, W. C. Li, A. H. Lu, *ACS Appl. Mater. Interfaces* **2012**, *4*, 6125–6132; b) G. P. Hao, W. C. Li, D. Qian, G. H. Wang, W. P. Zhang, T. Zhang, A. Q. Wang, F. Schüth, H. J. Bongard, A. H. Lu, *J. Am. Chem. Soc.* **2011**, *133*, 11378–11388.
- [5] a) B. Wang, A. P. Côté, H. Furukawa, M. O'Keeffe, O. M. Yaghi, *Nature* **2008**, *453*, 207–211; b) J. An, S. J. Geib, N. L. Rosi, *J. Am. Chem. Soc.* **2010**, *132*, 38–39.
- [6] a) X. L. Ma, X. X. Wang, C. S. Song, *J. Am. Chem. Soc.* **2009**, *131*, 5777–5783; b) S. Cui, W. W. Cheng, X. D. Shen, M. H. Fan, A. Russell, Z. W. Wu, X. B. Yi, *Energy Environ. Sci.* **2011**, *4*, 2070–2074.
- [7] a) F. S. Su, C. Y. Lu, *Energy Environ. Sci.* **2012**, *5*, 9021–9027; b) S. Choi, J. H. Drese, C. W. Jones, *ChemSusChem* **2009**, *2*, 796–854.
- [8] a) V. Presser, J. M. Donough, S. H. Yeon, Y. Gogotsi, *Energy Environ. Sci.* **2011**, *4*, 3059–3066; b) M. Sevilla, A. B. Fuertes, *Energy Environ. Sci.* **2011**, *4*, 1765–1771; c) V. Chandra, S. U. Yu, S. H. Kim, Y. S. Yoon, D. Y. Kim, A. H. Kwon, M. Meyyappan, K. S. Kim, *Chem. Commun.* **2012**, *48*, 735–737; d) M. C. Gutiérrez, D. Carriazo, C. O. Ania, J. B. Parra, M. L. Ferrer, F. D. Monte, *Energy Environ. Sci.* **2011**, *4*, 3535–3544; e) T. Ben, Y. Q. Li, L. K. Zhu, D. L. Zhang, D. P. Cao, Z. H. Xiang, X. D. Yao, S. L. Qiu, *Energy Environ. Sci.* **2012**, *5*, 8370–8376; f) L. Zhao, Z. Bacsik, N. Hedin, W. Wei, Y. H. Sun, M. Antonietti, M. M. Titirici, *ChemSusChem* **2010**, *3*, 840–845; g) S. Mazumder, P. van Hemert, A. Busch, K.-H. Wolf, P. Tejeracuesta, *Int. J. Coal Geol.* **2006**, *67*, 267–279.
- [9] a) T. Hasell, S. Y. Chong, K. E. Jelfs, D. J. Adams, A. I. Cooper, *J. Am. Chem. Soc.* **2012**, *134*, 588–598; b) T. Ben, H. Ren, S. Q. Ma, D. P. Cao, J. H. Lan, X. F. Jing, W. C. Wang, J. Xu, F. Deng, J. M. Simmons, S. L. Qiu, G. S. Zhu, *Angew. Chem.* **2009**, *121*, 9621–9624; *Angew. Chem. Int. Ed.* **2009**, *48*, 9457–9460.
- [10] a) A. Stein, Z. Y. Wang, M. A. Fierke, *Adv. Mater.* **2009**, *21*, 265–293; b) C. D. Liang, Z. J. Li, S. Dai, *Angew. Chem.* **2008**, *120*, 3754–3776; *Angew. Chem. Int. Ed.* **2008**, *47*, 3696–3717; c) Y. D. Xia, Z. X. Yang, R. Mokaya, *Nanoscale* **2010**, *2*, 639–659; d) R. E. Morris, P. S. Wheatley, *Angew. Chem.* **2008**, *120*, 5044–5059; *Angew. Chem. Int. Ed.* **2008**, *47*, 4966–4981; e) Z. Yong, V. G. Mata, A. E. Rodrigues, *Adsorption* **2001**, *7*, 41–50.
- [11] C. Pevida, T. C. Drage, C. E. Snape, *Carbon* **2008**, *46*, 1464–1474.
- [12] a) C. Pevida, M. G. Plaza, B. Arias, J. Feroso, F. Rubiera, J. J. Pis, *Appl. Surf. Sci.* **2008**, *254*, 7165–7172; b) M. G. Plaza, F. Rubiera, J. J. Pis, C. Pevida, *Appl. Surf. Sci.* **2010**, *256*, 6843–6849; c) J. Przepiński, M. Krodzewicz, A. W. Morawski, *Appl. Surf. Sci.* **2004**, *225*, 235–242; d) M. M. Maroto-Valer, Z. Tang, Y. Zhang, *Fuel Process. Technol.* **2005**, *86*, 1487–1542; e) C. C. Hwang, Z. Jin, W. Lu, Z. Z. Sun, L. B. Alemany, J. R. Lomeda, J. M. Tour, *ACS Appl. Mater. Interfaces* **2011**, *3*, 4782–4786; f) L. Liu, Q. F. Deng, T. Y. Ma, X. Z. Lin, X. X. Hou, Y. P. Liu, Z. Y. Yuan, *J. Mater. Chem.* **2011**, *21*, 16001–16009; g) J. A. Thote, K. S. Iyer, R. Chatti, N. K. Labhsetwar, R. B. Biniwale, S. S. Rayalu, *Carbon* **2010**, *48*, 396–402; h) C. Chen, J. Kim, W. S. Ahn, *Fuel* **2012**, *95*, 360–364; i) M. Sevilla, A. B. Fuertes, *J. Colloid Interface Sci.* **2012**, *366*, 147–154; j) W. Xing, C. Liu, Z. Y. Zhou, L. Zhang, J. Zhou, S. P. Zhuo, Z. F. Yan, H. Gao, G. Q. Wang, S. Z. Qiao, *Energy Environ. Sci.* **2012**, *5*, 7323–7327; k) M. Sevilla, P. Valle-Vigón, A. B. Fuertes, *Adv. Funct. Mater.* **2011**, *21*, 2781–2787; l) H. K. Youn, J. Kim, G. Chandrasekar, H. Jin, W. S. Ahn, *Mater. Lett.* **2011**, *65*, 1772–1774.
- [13] S. Builes, T. Roussel, C. M. Ghimbeu, J. Parmentier, R. Gadiou, C. Vix-Guterl, L. F. Vega, *Phys. Chem. Chem. Phys.* **2011**, *13*, 16063–16070.
- [14] L. F. Wang, R. T. Yang, *J. Phys. Chem. C* **2012**, *116*, 1099–1106.
- [15] a) B. Grzyb, C. Hildenbrand, S. Berthon-Fabry, D. Bégin, N. Job, A. Rigacci, P. Achard, *Carbon* **2010**, *48*, 2297–2307; b) J. Silvestre-Albero, A. Wahby, A. Sepulveda-Escribano, M. Martínez-Escandell, K. Kanekob, F. Rodríguez-Reinoso, *Chem. Commun.* **2011**, *47*, 6840–6842.
- [16] Z. S. Zhang, J. Zhou, W. Xing, Q. Z. Xue, Z. F. Yan, S. P. Zhuo, S. Z. Qiao, *Phys. Chem. Chem. Phys.* **2013**, *15*, 2523–2529.
- [17] A. Wahby, J. M. Ramos-Fernández, M. Martínez-Escandell, A. Sepulveda-Escribano, J. Silvestre-Albero, F. Rodríguez-Reinoso, *ChemSusChem* **2010**, *3*, 974–981.
- [18] a) A. H. Lu, W. C. Li, Z. S. Hou, F. Schüth, *Chem. Commun.* **2007**, 1038–1040; b) A. H. Lu, W. C. Li, E. L. Salabas, B. Spliethoff, F. Schüth, *Chem. Mater.* **2006**, *18*, 2086–2094.
- [19] T. E. Rufford, D. Hulicova-Jurcakova, K. Khosla, Z. H. Zhu, G. Q. Lu, *J. Power Sources* **2010**, *195*, 912–918.
- [20] a) D. Yothun, N. Vural, H. Demiral, *Microporous Mesoporous Mater.* **2009**, *122*, 189–194; b) K. Mohanty, M. Jha, B. C. Meikap, M. N. Biswas, *Ind. Eng. Chem. Res.* **2005**, *44*, 4128–4138.
- [21] a) H. L. Jiang, B. Liu, Y. Q. Lan, K. Kuratani, T. Akita, H. Shioyama, F. Q. Zong, Q. Xu, *J. Am. Chem. Soc.* **2011**, *133*, 11854–11857; b) L. Zhang, Y. H. Hu, *J. Phys. Chem. C* **2010**, *114*, 2566–2574.
- [22] a) S. J. Yang, T. Kim, J. H. Im, Y. S. Kim, K. Lee, H. Jung, C. R. Park, *Chem. Mater.* **2012**, *24*, 464–470; b) B. Liu, H. Shioyama, T. Akita, Q. Xu, *J. Am. Chem. Soc.* **2008**, *130*, 5390–5391.
- [23] a) C. F. Martín, M. G. Plaza, J. J. Pis, F. Rubiera, C. Pevida, T. A. Centeno, *Sep. Purif. Technol.* **2010**, *74*, 225–230; b) F. Stoeckli, M. V. López-Ramón, D. Hugi-Cleary, A. Guillot, *Carbon* **2001**, *39*, 1115–1116.
- [24] Y. Y. Liu, J. Wilcox, *Environ. Sci. Technol.* **2012**, *46*, 1940–1947.
- [25] Y. Zhao, Y. M. Shen, L. Bai, R. J. Hao, L. Y. Dong, *Environ. Sci. Technol.* **2012**, *46*, 1789–1795.
- [26] a) J. Jagiello, W. Betz, *Microporous Mesoporous Mater.* **2008**, *108*, 117–122; b) D. Gozzi, A. Latini, M. Tomellini, *J. Phys. Chem. C* **2009**, *113*, 45–53.

Received: June 18, 2013

Revised: July 30, 2013

Published online on October 2, 2013